

This is the accepted manuscript made available via CHORUS. The article has been published as:

Drexhage's Experiment for Sound

Lutz Langguth, Romain Fleury, Andrea Alù, and A. Femius Koenderink

Phys. Rev. Lett. **116**, 224301 — Published 2 June 2016

DOI: [10.1103/PhysRevLett.116.224301](https://doi.org/10.1103/PhysRevLett.116.224301)

The Drexhage experiment for sound

Lutz Langguth,¹ Romain Fleury,² Andrea Alù,^{1,2} and A. Femius Koenderink^{1,*}

¹*Center for Nanophotonics, FOM Institute AMOLF,*

Science Park 104, 1098 XG Amsterdam, The Netherlands

²*Department of Electrical and Computer Engineering, The University of Texas at Austin,
1616 Guadalupe Street, UTA 7.215, Austin, TX 78712, USA*

(Dated: May 4, 2016)

Abstract

Drexhage's seminal observation that spontaneous emission rates of fluorophores vary with distance from a mirror uncovered the fundamental notion that a source's environment determines radiative linewidths and shifts. Further, this observation established a powerful tool to determine fluorescence quantum yields. We present the direct analogue for sound. We demonstrate that a Chinese gong at a hard wall experiences radiative corrections to linewidth and lineshift, and extract its intrinsic radiation efficiency. Beyond acoustics, our experiment opens new ideas to extend the Drexhage experiment to metamaterials, nano-antennas, and multipolar transitions.

8 In 1968, Drexhage reported a seminal experiment [1, 2]: he demonstrated that the spontaneous
 9 emission decay rate of a fluorophore varies when its position in front of a mirror is varied on the
 10 scale of half a wavelength. This results from the back-action of the mirror through reflection of the
 11 emitted field [3, 4]. Equivalently, the effect can be described as the variation in the local density
 12 of optical states (LDOS) caused by the mirror [5]. This experiment has spawned an entire field of
 13 radiation engineering, including photonic band gaps to suppress LDOS [6], the use of microcav-
 14 ities to boost Purcell effects [7], and more recently plasmonics [8]. Aside from acting on decay
 15 rates, corresponding to the imaginary part of the transition frequency, the reflector back-action
 16 can also modify its real part, inducing a resonance shift [9, 10]. Aside from these fundamental
 17 cavity-QED implications, Drexhage’s experiment also stands out for practical purposes. Since
 18 back-action only affects radiative damping, and not competing non-radiative decay channels, the
 19 contrast of the variation in rate yields a direct measure of the emitter quantum efficiency [2, 3, 11–
 20 18]. Contrary to any other method to find quantum efficiencies, this measurement requires no
 21 absolute intensity data, nor trust in a reference standard. While in principle any LDOS variation
 22 may be used, Drexhage’s planarized geometry is the only one controlled sufficiently to be a prac-
 23 tical calibration tool. It has therefore been applied to determine quantum efficiencies of ensembles
 24 of molecules [2], rare earth ions [11, 12], quantum dots [14, 17, 19], single molecules [16], NV
 25 centers [18], and nano-antennas [16, 20].

26 In this work we present a time-domain version of Drexhage’s experiment for a classical audible
 27 acoustic source. We use a Chinese gong placed in front of a concrete wall that acts as reflec-
 28 tor. While originally conceived as a didactic tool, the experiment provides new perspectives on
 29 the physics of sound emission and beyond, for instance in optics of metamaterials, and multipole
 30 transitions. Inspecting the spectrum of the acoustic transient response after the gong is hit, one
 31 can conveniently analyze several resonant modes at the same time, highlighting crucial differ-
 32 ences between optical and acoustic Drexhage experiments. Classical acoustic textbooks predict
 33 that the radiation resistance of acoustic monopoles and multipoles varies in front of a reflective
 34 wall [21–25]. Yet, measurement of this effect to our knowledge has been proposed only based on
 35 cumbersome angle-resolved measurements of the radiation pattern that is numerically integrated
 36 to obtain a relative measure of total radiated power [26]. On the contrary, we directly measure
 37 the variation of radiation resistance from the spectral properties of the gongs’ ring-down. More-
 38 over, we also present a radiative shift analogous to radiative shifts in optics, or radiative *reactance*
 39 effects for antennas, yet entirely unforeseen in acoustics. In this sense, our experiment is to our

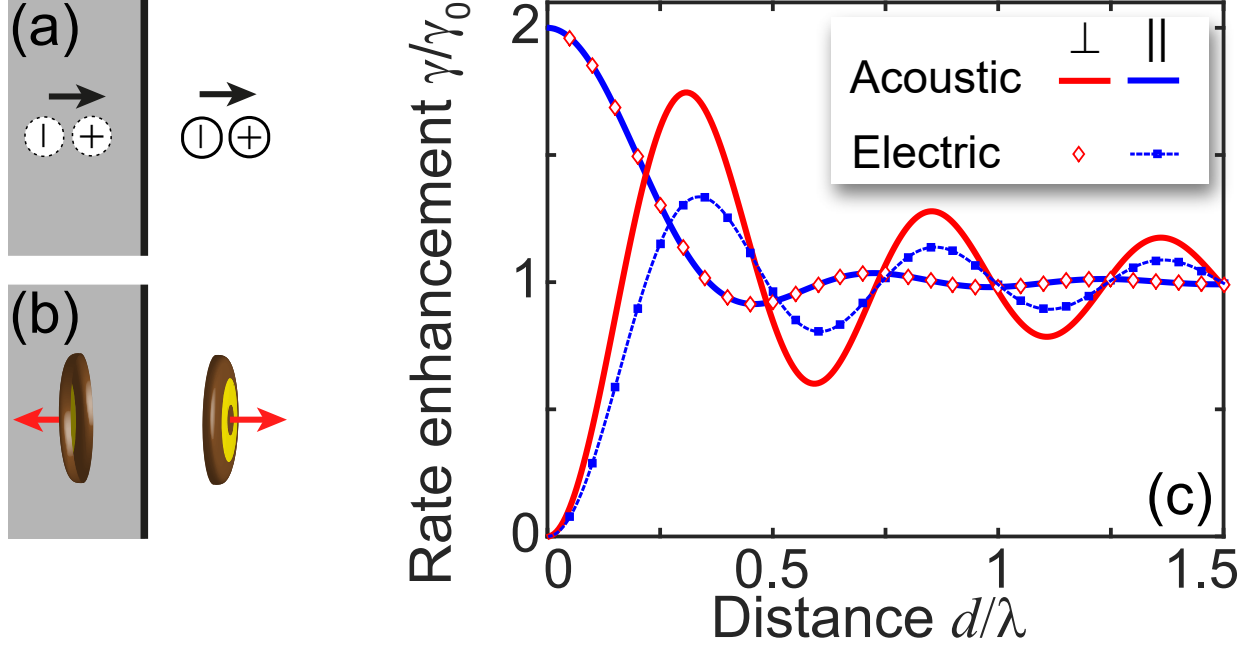


FIG. 1. (a) Image charge construction in optics for a vertical dipole above a mirror. (b) In acoustics, the mirror gong is not along, but opposite to, the source gong. Panel (c) shows the decay rate enhancement predicted by image theory for an acoustic dipole perpendicular to (red), and parallel to the interface (blue). The black symbols and thin line show the electrodynamic case.

knowledge unique as a direct demonstration of both radiative linewidth and lineshift modulation of an acoustic resonator source that is quantitatively explained by back-action. By analogy to optics, our experiment provides a simple, calibration-free method to quantitatively extract intrinsic radiation efficiencies of acoustic resonators. Such easy measurements of radiation efficiency can be used as calibration for the viscoelastic damping of materials, which is cumbersome to obtain in conventional measurement schemes [27].

Before discussing our experiment it is instructive to revisit how Drexhage described fluorescence lifetime variations in front of a mirror [1–3, 28]. The classical electrodynamic analogue of the change in fluorescence decay rate is the change in total power that an oscillating electric dipole of fixed current radiates. In presence of a perfectly conducting (electric) mirror, image charge analysis (Fig. 1) applies. The field at an observation point $\mathbf{R} = R(\cos \theta, \sin \theta)$, with $R \gg \lambda$ reads

$$\mathbf{E}(\mathbf{R}) \approx \frac{e^{ikR}}{R} \mathbf{S}(\theta, \phi) [e^{ik \cos \theta d} + q e^{-ik \cos \theta d}], \quad (1)$$

given a source emitting at frequency $\omega = ck$, placed a distance d from the mirror. Two essential ingredients determine the overall radiation features: first, the amplitude and sign q of the image

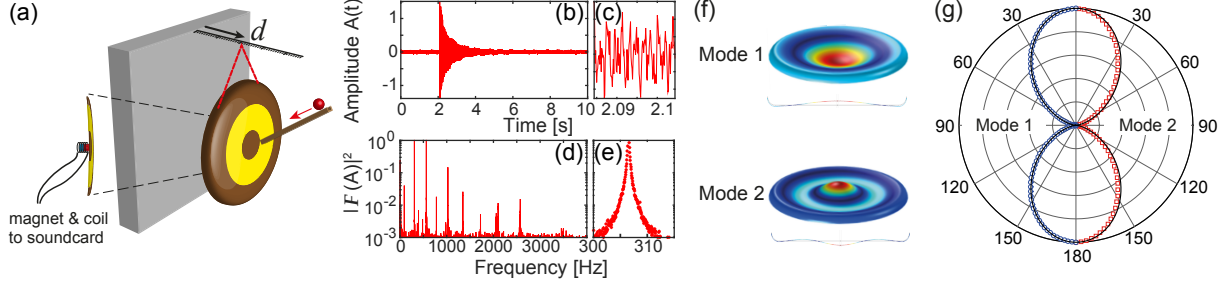


FIG. 2. (a) Sketch of the experiment. A wooden ball launched on a rail generates a δ -excitation at the gong center. The gong displacement is picked up by a small magnet glued to the back of the gong, and a pick-up coil. Panel b (zoom in c) shows a time-domain trace, showing a ring down with many frequency components. Panel d: the Fourier transform of the transient shows distinct resonances. The main resonances (zoom shown for mode 1, 306 Hz in panel e) have a Lorentzian lineshape. (f) Acoustic eigenmode profile for Mode 1 and 2, the lowest order modes of zero angular quantum number. (g) Far field radiation patterns for the gong in free space for modes 1 (blue circles, FEM result) and 2 (red squares, FEM result) indicate dipole-like emission (black curves indicating $\cos^2 \theta$). In terms of integrated radiated flux for mode 1 and mode 2, resp. over 99% and 95% are in the dipole mode.

dipole, and second the radiation pattern $S(\theta, \phi)$. When transposing this analysis to acoustics, two considerations are important. First, the reflection coefficient of a hard wall has opposite sign compared to an electric mirror. In other words, while electric fields have a node at a mirror, pressure waves have an anti-node. Consequently, mirror dipoles have opposite signs q for the electric and acoustic case (Figure 1a versus b). A second crucial difference is that acoustic radiation patterns $S(\theta, \phi)$ are strongest along the dipole axis ($\cos^2 \theta$ pattern) exactly opposite to the $\sin^2 \theta$ behavior in optics. Integrating the radiated power over the half space above the mirror results in the acoustic equivalent to Drexhage formulas

$$\begin{aligned} \frac{\gamma_{\perp}(x)}{\gamma_{\infty}} &= 1 + \eta \left[-\frac{3 \sin(x)}{x} - \frac{6 \cos(x)}{x^2} + \frac{6 \sin(x)}{x^3} \right] \\ \frac{\gamma_{\parallel}(x)}{\gamma_{\infty}} &= 1 + \eta \left[-\frac{3 \cos(x)}{x^2} + \frac{3 \sin(x)}{x^3} \right] \end{aligned} \quad (2)$$

with $x = 2kd = 4\pi d/\lambda$, and η denoting the acoustic radiation efficiency [29]. Here $\gamma_{\perp, \parallel}$ denotes the linewidth for dipole orientation perpendicular resp. parallel to the mirror and γ_{∞} is the linewidth in absence of the mirror. Morse and Ingard list expressions similar to Eq. (2), with $\eta = 1$, for the radiation impedance of an acoustic dipole [21, 22] at a hard wall. As in optics, at zero distance we find zero and double radiated power (assuming $\eta = 1$), indicating complete

destructive or constructive interference between source and image, depending on source dipole orientation. However, due to the opposite image charge sign, the sign of the oscillations is reversed. Full cancellation occurs for acoustic dipoles perpendicular to the wall, while in electromagnetics it requires dipoles *along* the mirror. For this scenario (red line in Fig. 1c), as one moves away from the reflector the contrast in oscillations is much stronger for sound than light, due to the different radiation patterns.

For our experiment we used a widely available Chinese ‘Chao’ gong, a slightly convex round brass plate of 0.5 mm thickness and 10 cm radius, and a turned up rim. The gong is suspended with string from a frame. A reproducible excitation is obtained by a wooden sphere (diameter ≈ 1 cm) rolling down a rail, hitting the gong approximately in the middle (Fig. 2a). To pick up the gong response, a small magnet was glued on the backside, again in the center of the gong. The magnet induces a current in a pickup coil that was recorded by a laptop sound card with 8 kHz sampling rate. Gongs have a plethora of modes with varying radial and azimuthal quantum number, forming an exciting platform for generalized Drexhage experiments. In this Letter we select modes with azimuthal order $m = 0$, since excitation and measurement are at the center. We recorded transients of 20 seconds, long enough to observe the full ring-down (Fig. 2b,c). We recorded a total of 80 acoustic ring-downs for distances to a concrete wall ranging from 7.5 to 120 cm. For each measured transient, we computed the Fourier spectrum (Fig. 2d,e), finding 9 distinct resonances between 300-3500 Hz, in addition to a ca. 1 Hz signal, associated with the small, ca. 1mm amplitude swinging motion of the gong due to being hit by the sphere. Here we focus on the two lowest frequency modes, observed at 306 and 561 Hz. According to finite-element simulations discussed further below, the mechanical deformation (Fig. 2f) for the lowest frequency $m = 0$ eigenmode corresponds to the ‘drum’ acoustic mode, while the second mode has two radial nodes. Both modes have an almost dipolar far-field radiation pattern with dipole moment normal to the gong (Fig. 2g).

For both gong modes we fit a Lorentzian to the peaks identified in the Fourier-transformed transients to find resonance frequency f , and damping rate γ , plotted in Fig. 3 as function of the separation between the gong and the wall. The linewidth clearly displays a characteristic oscillation resembling that of the fluorescence lifetime in the original Drexhage experiment. For the first mode (306 Hz, Q of 1200) we find ≈ 2 oscillations in the measured distance range which reduce in amplitude with increasing distance. At the shortest distance of 7.5cm the decay rate reduces by $\approx 8\%$, while at $z_0 = 35$ cm it increases by 7% relative to the natural linewidth.

89 For the second mode (561 Hz, $Q = 860$) we observe more oscillations in the same distance
 90 range, commensurate with the shorter acoustic wavelength. Further, these oscillations have larger
 91 contrast, indicating a higher radiation efficiency. Similar to the case of optical emitters with sub-
 92 unity quantum efficiency, the contrast in the Drexhage oscillations is not as large as expected for
 93 an ideal gong according to Figure 1. Indeed, back-action only affects the radiative damping rate,
 94 and not any other intrinsic nonradiative decay. As in optics, this can be captured defining the
 95 radiation efficiency η , already introduced in Eq. (2). While in acoustics with ‘radiation efficiency’
 96 one sometimes means comparison of radiated power to some reference object [30], here we intend
 97 the term as an absolute measure, i.e. as the ratio between total energy that the gong mode emits
 98 as sound to the total energy contained in the mode. This definition for acoustics [31] is analogous
 99 to the radiative efficiency definition for antennas [32] and to the radiative quantum efficiency of a
 100 fluorophore. Lines in Figure 3 show the image-theory prediction overplotted with the data, with as
 101 adjustable parameter the radiation efficiency (note that γ_∞ can be separately measured in absence
 102 of the wall). We find excellent agreement for fitted radiation efficiencies of $\eta = 9.5\%$ and 20%
 103 for the first and second gong mode, respectively. This radiation efficiency is a property of the
 104 gong modes, and not of their excitation or detection, and results from viscoelastic damping in the
 105 brass. The excellent fit further indicates that, while the gong is lossy, the wall is much closer to
 106 an ideal reflector than a silver mirror in optics. We note that non-ideal wall reflection (amplitude
 107 coefficient r) can be approximately included in Eq. (1) by reducing $|q|$ to $|r|$, leading to a reduction
 108 in oscillation contrast by a factor $1 - (1 - |r|)^2$ (negligibly different from unity for concrete).

109 In optics the frequency shift of radiative transitions near mirrors has been a longstanding topic
 110 of research [4, 33–35]. In principle, back-action should cause frequency shifts of the same or-
 111 der of magnitude as the decay rate change. Since in optics one deals with MHz decay rates,
 112 radiative lineshifts cannot be realistically observed, except for atoms [9, 10, 33, 35, 36]. In these
 113 systems, however, various quantum-mechanical effects contribute to lineshifts, so apart from how
 114 to measure shifts, also how to separate quantum-mechanical and classical contributions has been
 115 debated [4, 33–35]. Attempts to measure radiative lineshifts with optical scatterers as opposed to
 116 emitters provide the advantage of large intrinsic radiative lineshifts [37] but are compounded by
 117 the difficulty of correcting for spatial variations in the standing wave driving fields. Our acoustic
 118 measurement represents an ideal testbed to experimentally observe these effects. Indeed our mea-
 119 surement shows a clear red shift for short distances (< 0.2 m) between gong and reflector that is
 120 fully explained by interaction of the gong with its mirror image.

Mathematically, the radiative lineshift cannot be obtained by assuming fixed-frequency driving, and performing a radiation pattern integral [38], as done to derive Eq. (2). Instead, consider a small acoustic oscillator of resonance frequency ω_0 with displacement coordinate \mathbf{u} that carries dipole moment $\mathbf{D}(t) = \rho/(4\pi)\mathbf{W}\ddot{\mathbf{u}}(t)$ (where ρ is the background density and \mathbf{W} is the entrained mass tensor). We analyze back-action by subjecting the oscillator (intrinsic damping from loss plus radiation γ_∞) to the force $\mathbf{F}_s(t)$ from its own mirror image

$$\ddot{\mathbf{u}} + \gamma_\infty \dot{\mathbf{u}} + \omega_0^2 \mathbf{u} = \mathbf{F}_s(t)/m.$$

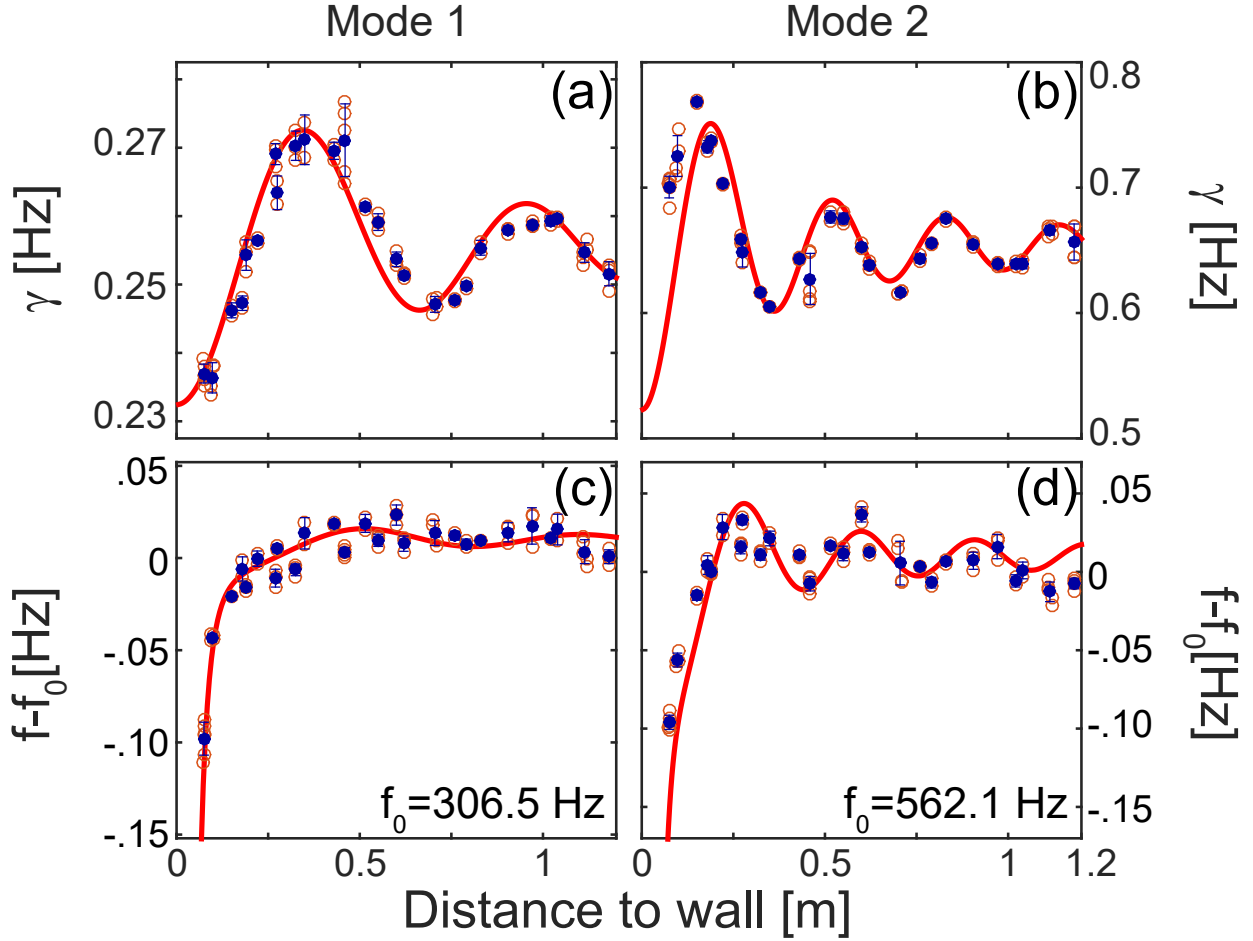


FIG. 3. (a,b) Fitted damping rate for Mode 1 (306 Hz) and Mode 2 (561 Hz) versus distance to the wall. Open orange points indicate individual measurement points, while solid blue ones shows their averages, binned in 5 cm intervals. Overplotted is Eq. 2 with parameters $\gamma_\infty = 0.255$ Hz and $\eta = 0.09$, resp. $\gamma = 0.654$ Hz and $\eta = 0.20$. Panels (c,d) show the lineshift for each mode, where the theory contains *no* further adjustable parameters.

The Ansatz $[\mathbf{u}(t), \mathbf{F}(t)] = [\mathbf{u}_0, \mathbf{F}_0] e^{-i(\omega_0 + \Delta\omega)t - \gamma/2t}$ results in (assuming $\Delta\omega \ll \omega_0$)

$$\Delta\omega = -\frac{\text{Re}\left\{\mathbf{u}_0^\dagger \cdot \mathbf{F}_0\right\}}{2m\omega_0 u_0^2} \quad \text{and} \quad \gamma = \gamma_\infty + \frac{\text{Im}\left\{\mathbf{u}_0^\dagger \cdot \mathbf{F}_0\right\}}{m\omega_0 u_0^2}.$$

Since the force \mathbf{F}_0 is linear in displacement \mathbf{u}_0 , the frequency shift $\Delta\omega$ and decay rate change are amplitude-independent. Through $\mathbf{F}_0 \propto \mathbf{G}(\mathbf{r}, \mathbf{r}) \cdot \mathbf{u}_0$, in the decay rate change we recognize the imaginary part of the Green function $\mathbf{G}(\mathbf{r}, \mathbf{r}')$, known as LDOS in optics, which in energy balance terms appears when one evaluates how much work the displacement does against the force from its own mirror image. Likewise, the real part of the Green function enters the lineshift. For a perfect mirror, an image dipole approach for \mathbf{F}_0 predicts

$$\begin{aligned} \frac{\Delta\omega_\perp(x)}{\gamma_\infty} &= \eta \left[\frac{3 \cos(x)}{2x} - \frac{3 \sin(x)}{x^2} - \frac{3 \cos(x)}{x^3} \right] \\ \frac{\Delta\omega_\parallel(x)}{\gamma_\infty} &= -\eta \left[\frac{3 \sin(x)}{2x^2} + \frac{3 \cos(x)}{2x^3} \right]. \end{aligned} \quad (3)$$

As in optics [4, 29, 33, 35], close to the mirror the resonance will red shift, meaning the mirror image provides driving along the displacement. Returning to our experiment, all the parameters required to compare the measured frequency shift with the predicted one are already fully determined by the fit to the measured oscillation in damping rate. Overplotting the prediction from Eq. (3) with the measured shift shows excellent correspondence. In other words, the measured lineshift is completely consistent with the back-action interaction of the gong with its own reflection.

To further validate our results, and provide further insights, we consider finite-element (FEM, COMSOL Multiphysics) simulations for Mode 1 with single radial antinode, and the higher Mode 2 [43]. These eigenmodes have a dominant dipole character (Fig. 2(f,g)), validating our assumptions in the above theory. Simulations for an ideally elastic, lossless brass gong in front of a solid wall predicts that both linewidth and center frequency [38] closely follow the image charge prediction Eqs. (2,3) with $\eta = 1$, as shown in Figure 4(a,b) [38]. The agreement is especially good (percent-level) for Mode 1, while for Mode 2 there is a small deviation that can be captured as an apparent offset of about $\lambda/20$ in the distance axis. We attribute this to the fact that for Mode 2 the gong is not very small compared to the wavelength (gong diameter about $\lambda/3$). In simulations for various viscoelastic loss tangents $\tan \delta = \text{Im}E/\text{Re}E$ (with E the complex Young modulus), we find smaller linewidth variations that are well captured by image theory taking $\eta < 1$. As exemplified for Mode 1 in Figure 4(c), we find excellent correspondence taking a relation between

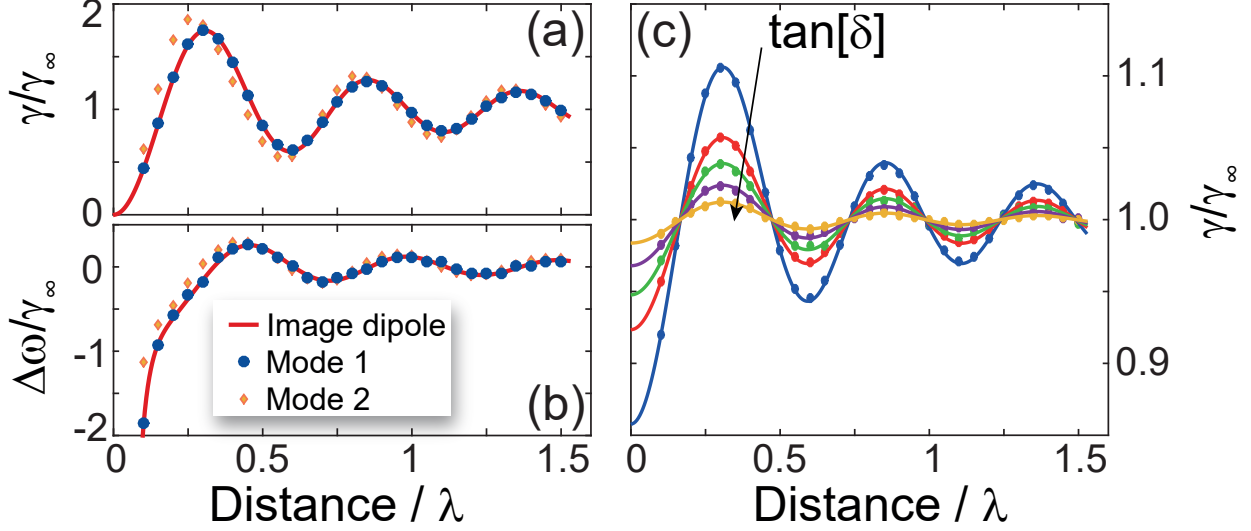


FIG. 4. (a,b) Linewidth and lineshift normalized to the linewidth in free space of mode 1, assuming no viscoelastic damping. Dark circles (light diamonds) are for mode 1 and 2 respectively, from FEM. Solid line is the image theory prediction, (c) Points show finite element simulations of the linewidth for loss tangents $\tan \delta = 0.1, 0.2, 0.3, 0.5$ and 1.0×10^{-4} . Lines show Eq. (2) with radiation efficiencies of $\eta = 14.2, 7.6, 5.2, 3.2$ and 1.6% .

radiation efficiency and material of the form $\eta = 1/(1 + \kappa \tan \delta)$, where $\kappa^{-1} = 0.165 \cdot 10^{-5}$ is a mode-dependent parameter. Interestingly, the Drexhage experiment yields a radiation efficiency that directly maps onto a calibration of viscoelastic damping. For instance, assuming the FEM geometry accurately represents our gong, the measured $\eta = 0.09$ (Mode 1) translates into a loss tangent of $1.6 \cdot 10^{-4}$ at 306 Hz, reasonable for brass alloys. This provides an upper bound, as the gong suspension and readout may also impart loss. Using a less resistive coil or circuit, or all-optical sensing can reduce this loss. Compared to measuring viscoelastic damping using calibrated time-harmonic stress-strain measurements [27] this method is extremely simple. A frequency series could be mapped using multipolar modes, or a set of resonators. Sound absorption in the wall that is used as reflector has only a small effect on the apparent radiation efficiency. For instance, including realistic acoustic loss of concrete in the simulations shows only a $< 0.1\%$ difference. The key is that absorption does not preclude extremely large impedance mismatch, ensuring near-unity reflection constant. We refer to the supplement [38] for a comparative analysis of wall non-idealities.

To conclude, we demonstrated the acoustic analogue of Drexhage's seminal experiment, finding

155 both a back-action induced change in damping and resonance frequency. This experiment is firstly
 156 an object lesson in radiation reaction physics that is seminal in the study of spontaneous emission
 157 rates and radiative lineshifts in optics. A second important quality of the experiment is that it
 158 transposes Drexhage’s method as a calibration of radiation efficiency to sound. Generally, it is not
 159 trivial to determine the intrinsic radiation efficiency of an acoustic emitter. Most efficiency mea-
 160 surements require a calibrated comparison of how much excitation energy is loaded into a mode to
 161 total radiated output power. As in optics, an absolute measure of total radiated power is difficult,
 162 as one needs calibrated detectors that capture all solid angles. Regarding the driving, one notes
 163 that in the work of Lim [26] the electric driving circuit was implicitly *assumed* to yield constant
 164 acoustic source strength, whereas in fact any energy balance would need accounting for all electri-
 165 cal and mechanical losses. We speculate that the ability to simply measure radiation efficiency can
 166 also impact material characterization, by mapping radiation efficiency onto viscoelastic loss tan-
 167 gents. Finally, a third merit of our experiment is that it provides a perspective on generalizations of
 168 Drexhage’s experiment. Back-action depends on whether the source has electric dipole character,
 169 or maybe magnetic, chiral or multipolar moments, a fact pursued to understand magnetic dipole
 170 transitions in rare earth ions [44], quadrupole moments of quantum dots [15] and bianisotropic
 171 resonances in split rings [45]. Conversely, back-action can be used as a probe of unconventional
 172 boundary conditions that a reflector may provide, for instance when it is not a standard mirror, but
 173 a metamaterial, or metasurface [46, 47]. While a challenge in optics, Drexhage experiments with
 174 multipoles and metasurfaces can be readily explored in acoustics or radio-frequencies.

175 This work is part of the research program of the Foundation for Fundamental Research on
 176 Matter (FOM), which was financially supported by The Netherlands Organization for Scientific
 177 Research (NWO). This work was furthermore supported by NanoNextNL, a microtechnology and
 178 nanotechnology consortium of the Government of the Netherlands and 130 partners. AA was
 179 partially supported by a Visiting Professorship of the KNAW, the Royal Netherlands Academy of
 180 Arts and Sciences. RF acknowledges support from the Acoustical Society of America through
 181 the Frederick V. Hunt postdoctoral research fellowship in acoustics. AA and RF acknowledge the
 182 Air Force Office of Scientific Research grant No. FA9550-13-1-0204. L. Langguth and R. Fleury
 183 contributed equally to this work.

184 * f.koenderink@amolf.nl

- 185 [1] K. H. Drexhage, H. Kuhn, and F. P. Schäfer, Ber. Bunsen Phys. Chem. **72**, 329 (1968).
- 186 [2] K. Drexhage, J. Lumin. **1-2**, 693 (1970).
- 187 [3] R. R. Chance, A. Prock, and R. Silbey, Adv. Chem. Phys. **37**, 1 (1978).
- 188 [4] S. Haroche, in *Les Houches Session LIII 1990, Systèmes Fondamentaux en Optique Quantique:*
189 *Course 13, Cavity Quantum Electrodynamics* (Elsevier Science Publishers B.V., New York, 1992).
- 190 [5] H. Khosravi and R. Loudon, Proc. Roy. Soc. Lon. Series A **436**, 373 (1992).
- 191 [6] C. M. Soukoulis, ed., *Photonic Crystals and Light Localization in the 21st Century* (Kluwer Academic
192 Publishers, 2001).
- 193 [7] P. Lodahl, S. Mahmoodian, and S. Stobbe, Rev. Mod. Phys. **87**, 347 (2015).
- 194 [8] V. Giannini, A. Fernández-Domínguez, S. C. Heck, , and S. A. Maier, Chem. Rev. **111**, 3888 (2011).
- 195 [9] M. A. Wilson, P. Bushev, J. Eschner, F. Schmidt-Kaler, C. Becher, R. Blatt, and U. Dorner, Phys. Rev.
196 Lett. **91**, 213602 (2003).
- 197 [10] D. J. Heinzen and M. S. Feld, Phys. Rev. Lett. **59**, 2623 (1987).
- 198 [11] E. Snoeks, A. Lagendijk, and A. Polman, Phys. Rev. Lett. **74**, 2459 (1995).
- 199 [12] R. M. Amos and W. L. Barnes, Phys. Rev. B **55**, 7249 (1997).
- 200 [13] R. J. Walters, J. Kalkman, A. Polman, H. A. Atwater, and M. J. A. de Dood, Phys. Rev. B **73**, 132302
201 (2006).
- 202 [14] M. D. Leistikow, J. Johansen, A. J. Kettelarij, P. Lodahl, and W. L. Vos, Phys. Rev. B **79**, 045301
203 (2009).
- 204 [15] M. L. Andersen, S. Stobbe, A. S. Sørensen, and P. Lodahl, Nature Phys. **7**, 215 (2011).
- 205 [16] B. C. Buchler, T. Kalkbrenner, C. Hettich, and V. Sandoghdar, Phys. Rev. Lett. **95**, 063003 (2005).
- 206 [17] A. Kwadrin and A. F. Koenderink, J. Phys. Chem. C **116**, 16666 (2012).
- 207 [18] M. Frimmer, A. Mohtashami, and A. F. Koenderink, Appl. Phys. Lett. **102**, 121105 (2013).
- 208 [19] P. Lunnemann, F. T. Rabouw, R. J. A. van Dijk-Moes, F. Pietra, D. Vanmaekelbergh, and A. F.
209 Koenderink, ACS Nano **7**, 5984 (2013).
- 210 [20] M. Frimmer and A. F. Koenderink, Phys. Rev. Lett. **110**, 217405 (2013).
- 211 [21] P. M. Morse and K. U. Ingard, *Theoretical Acoustics* (Princeton University Press, Princeton, NJ, 1987).
- 212 [22] U. Ingard and G. Lamb jr., J. Acoust. Soc. Am **29**, 743 (1957).
- 213 [23] R. V. Waterhouse, J. Acoust. Soc. Am **35**, 1144 (1963).
- 214 [24] G. C. Maling jr., J. Acoust. Soc. Am **36**, 781 (1964).
- 215 [25] R. V. Waterhouse, J. Acoust. Soc. Am **36**, 783 (1964).

- [26] K. M. Lim, Appl. Acoust. **15**, 283 (1982).
- [27] R. S. Lakes, Rev. Sci. Instrum. **75**, 797 (2004).
- [28] K. H. Drexhage, Prog. Opt. **12**, 165 (1974).
- [29] The electromagnetic equivalents are $\gamma_{\perp}(x)/\gamma_{\infty} = 1 + 3\eta[-\cos(x)/x^2 + \sin(x)/x^3]$, and $\gamma_{\parallel}(x)/\gamma_{\infty} = 1 + 3\eta/2[-\sin(x)/x - \cos(x)/x^2 + \sin(x)/x^3]$, resp. $\delta\omega_{\perp}/\gamma_{\infty} = -3/2\eta[\sin(x)/x^2 + \cos(x)/x^3]$ and $\delta\omega_{\parallel}(x)/\gamma_{\infty} = 3/4\eta[\cos(x)/x - \sin(x)/x^2 - \cos(x)/x^3]$.
- [30] F. G. Leppington, E. G. Broadbent, and K. H. Heron, Proc. R. Soc. London, Ser. A **382**, 245 (1982).
- [31] S. Wu, ed., *Acoustic Radiation and Wave Propagation, Proceedings of the 1994 Symposium on Structure-Sound Interaction* (American Society of Mechanical Engineers (ASME) Press, New York, 1994).
- [32] IEEE Std 145-2013 (Revision of IEEE Std 145-1993). IEEE Standard for Definitions of Terms for Antennas , 1 (2014).
- [33] E. A. Hinds and V. Sandoghdar, Phys. Rev. A **43**, 398 (1991).
- [34] W. L. Barnes, J. Mod. Opt. **45**, 661 (1998).
- [35] D. Meschede and A. Schenzle, “Entangled Atoms and Fields: Cavity QED,” in *Handbook of Atomic, Molecular, and Optical Physics*, edited by G. W. F. Drake (Springer, 2006) p. 1167.
- [36] V. V. Ivanov, R. A. Cornelussen, H. B. van Linden van den Heuvell, and R. J. C. Spreeuw, J. Opt. B. **6**, 454 (2004).
- [37] W. R. Holland and D. G. Hall, Phys. Rev. Lett. **52**, 1041 (1984).
- [38] See Supplemental Material at [URL will be inserted by publisher], which includes Refs. [39–42], for technical details of the FEM implementation, a derivation of back-action in the vibro-acoustic problem, on basis of the gongs entrained mass tensor, and an analysis of the effect of nonideal reflectors.
- [39] A. D. Pierce, *Acoustics: An Introduction to Its Physical Principles and Applications* (Acoustical Society of America, Woodbury NY, 1991).
- [40] D. A. Russell, Am. J. Phys. **67**, 660 (1999).
- [41] M. J. Crocker, *Handbook of Acoustics* (John Wiley & Sons, New York, 1998).
- [42] L. Novotny and B. Hecht, *Principles of Nano-Optics* (Cambridge University Press, Cambridge, 2006).
- [43] FEM simulations including the magnet as a rectangular mass at the center of the gong show that, being centered, it does not impact the mode shape, but does detune the gong.
- [44] S. Karaveli and R. Zia, Phys. Rev. Lett. **106**, 193004 (2011).
- [45] A. Kwadrin and A. F. Koenderink, Phys. Rev. B **87**, 125123 (2013).

²⁴⁷ [46] J. Kästel and M. Fleischhauer, Phys. Rev. A **71**, 011804 (2005).

²⁴⁸ [47] R. Ruppin and O. J. F. Martin, J. Chem. Phys. **121**, 11358 (2004).